INTERNATIONAL ATOMIC ENERGY AGENCY
UNITED NATIONS EDUCATIONAL, SCIENTIFIC AND CULTURAL ORGANIZATION
INTERNATIONAL CENTRE FOR THEORETICAL PHYSICS
I.C.T.P., P.O. BOX 586, 34100 TRIESTE, ITALY, CABLE: CENTRATOM TRIESTE

H4.SMR/642 - 8

College on Methods and Experimental Techniques in Biophysics

28 September - 23 October 1992

New Directions in Protein Crystal Growth

C.E. BUGG

University of Alabama, U.S.A.

These are preliminary lecture notes, intended only for distribution to participants.

TIBTECH – JULY 1987 [Vol. 5]

REVIEWS

New directions in protein crystal growth

L. J. DeLucas and C. E. Bugg

Major advances in the technology involved in determining protein crystal structures have facilitated several new and existing applications for protein crystallography. Protein crystal growth, the one major bottleneck in this field, has recently received much attention and several new developments hold promise for the future.

Since completion of the first crystallographic study of a protein structure (myoglobin) in 1960[1], crystallography has become a valuable tool for determining the three-dimensional structures of complicated biomolecules. 'Protein crystallography', a term used widely to describe crystallographic studies of biological molecules such as proteins and nucleic acids[2,3] has played a key role in establishing the structural foundations of molecular biology and biochemistry. It has been important in revealing structure/function relationships that are of major importance in understanding how macromolecules operate in biological systems. Crystallographic studies of proteins have become of interest in the past few years to the pharmaceutical, biotechnology, and chemical industries, as promising tools in protein engineering, drug design and other applications to biological systems.

Other methods for determining protein structure, such as two-dimensional NMR spectroscopy which can be performed using proteins in solution, are likely to become more and more useful during the next few years, but it is unlikely that any of these techniques will be competitive with crystallography in the near future for routinely determining three-dimensional structures of large proteins and other complicated biological macromolecules. Unfortunately, protein crystallography has the unique requirement that relatively large, high-quality single crystals must be obtained before a structural study can be pursued. Therefore, protein crystal growth has become a topic of considerable importance.

In practice, all of the major steps that are involved in determining a protein structure by crystallographic techniques (see Fig. 1) are subject to a number of experimental difficulties. Most of the proteins that have been studied during the past three decades required many years of intense effort before the complete three-dimensional structure was known. Consequently, until recently, there was limited interest in using protein crystallography as a general tool in biological research, and protein crystallography programs were limited to a few laboratories, primarily in academic institutions.

The advent of recombinant DNA techniques, however, has made it easier and quicker to obtain suitable amounts of pure protein. Similarly, several recent advances in technology (i.e. synchrotron radiation sources, electronic area detectors, computer graphics, anomalous dispersion methods for determining protein phases, new refinement techniques and software) have made it much easier to determine the crystal structure of a protein or other macromolecules.

Significantly, these major advances involve those experimental steps which are undertaken either before or after suitable crystals have been obtained. For the most part, the general procedures that are used for growing protein crystals have not changed appreciably during the last few years. Most protein crystals are still grown by brute-force, trial-and-error methods, which require investigations of large numbers of experimental conditions in hopes of identifying those that will produce usable crystals. However, once good crystals of a particular protein have been obtained, the crystallography often moves along at a rapid rate.

Current techniques for protein crystal growth

Various techniques have been utilized to grow protein crystals[4]. In all of these methods, crystallization is dependent upon control of solubility, and on the kinetics of nucleation and subsequent growth. Solubility is influenced by inherent properties of the macromolecule itself as well as by its environment (i.e. solvent, temperature, pH etc.). In all the crystallization methods, the basic principle is that a condition of supersaturation of the protein solution is approached slowly, while trying to maximize favorable intermolecular interactions[4].

It is generally believed that the protein must be homogeneous and free of contaminants to optimize the chance of producing large high-quality crystals[4,5] and advances in purification techniques (i.e. HPLC, affinity chromatography, isoelectric focusing, etc) have been important. However, for many proteins of interest, it remains difficult to produce large quantities of purified material.

Micromethods

A major achievement in protein crystal growth technology has been the development of methods that permit crystal growth studies using

Lawrence DeLucas is at the Centre for Macromolecular Crystallography and Charles Bugg is at the Department of Biochemistry, University of Alabama, Birmingham, AL 35294, USA.

Fig. 1

A bottleneck in protein X-ray crystallography

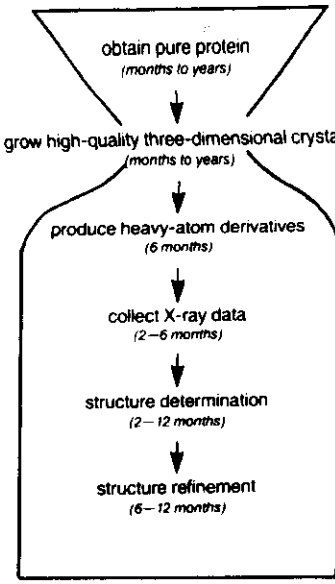

To determine the structure of a protein by crystallography, it is generally necessary to grow discrete single crystals for detailed X-ray diffraction studies (Fig. 5). These crystals usually must be about 0.3–1.0 mm on a side; considerably larger crystals are required for neutron diffraction studies. High-resolution data sets require accurate measurements for the intensities of thousands of diffraction profiles from crystals of the protein, typically referred to as 'native' protein crystals. Generally, heavy-atom derivatives (e.g. metal complexes or complexes that contain multi-electron atoms such as iodine) must be prepared, either by diffusing these complexes into the native protein crystals, or by crystallizing the macromolecule in the presence of the heavy-atom complexes. The techniques of multiple-isomorphous replacement[2], which have been widely used for solving protein structures, require that a series of different heavy-atom complexes must bind to the protein without disrupting the native crystal-packing scheme. Once potential derivatives are identified and diffraction data sets recollected for each of the heavy-atom complexes, an electron density map is calculated. Finally, a protein model that matches the map is constructed and refined, by adjusting atomic parameters so that the calculated diffraction patterns agree with the measured data.

microliter quantities of sample: these include dialysis, liquid–liquid diffusion and vapor-diffusion.

Dialysis. In the dialysis technique, the protein solution is held within a small chamber by a semipermeable membrane. The protein solution is then slowly brought toward a state of supersaturation by dialysis against an external solution containing a precipitating agent[4,6]. Crystal growth conditions can be adjusted easily by controlling the composition of the external solution (i.e. precipitant concentration, pH, buffer type, etc). Microliter quantities of sample in specially constructed dialysis cells[4,6], can be used for screening potential crystallization conditions and unsuccessful experiments (precipitated samples) can often be repeated by modification of the external solution. Another advantage of the dialysis method is that as the difference in concentrations inside and outside the dialysis cell decreases, so too does the rate of equilibration, thereby permitting a gradual asymptotic approach to equilibrium.

Liquid–liquid diffusion. Crystallization by free interface liquid–liquid diffusion is similar to dialysis except that two solutions (protein and precipitant) are not separated by a semipermeable membrane. One is layered on top of the other (typically the more dense solution is placed at the bottom) and allowed to diffuse until equilibrium is reached. The high protein and precipitant concentrations initially present at the interface create conditions suitable for crystal nucleation. As diffusion continues, the lower protein and precipitant concentrations favor optimal crystal growth from pre-existing nuclei[7,8].

Vapor diffusion. The technique that is now most widely used for protein crystal growth involves equilibration by vapor diffusion. Droplets of protein solution (as small as 0.5 μl) containing concentrations of precipitant slightly below that needed to render the protein insoluble, are placed over reservoirs containing higher precipitant concentrations. The droplet then slowly equilibrates with the reservoir through the vapor phase. The process is typically used for screening large numbers of conditions by placing the protein droplets on siliconized coverslips, which are subsequently inverted (to give hanging drops) and placed over small (1 ml) reservoirs in multi-chamber plates. Several hundred combinations of pH, buffer type, precipitant type, precipitant concentration, temperature, etc. can be examined quickly by this approach using only a few milligrams of protein.

Major problems in protein crystal growth

Despite the development of standard micromethods for crystallizing biological materials, protein crystal growth has continued to be much more of an art than a science. Generally, suitable crystals are obtained only by screening procedures that involve examination of hundreds or thousands of experimental conditions. Generally, protein concentrations ranging between 5 and 50 mg/ml are used with initial experiments performed at room temperature (≈22°C) and/or 4°C. The pH and ionic strength is varied using a variety of buffers and salts; initial pH screenings extend from pH = 2.0 to pH = 10.0. Finally, precipitating agents include salts such as NaCl or NH_4SO_4 and organic compounds such as hexylene glycol (2-methyl-2,4-pentanediol) and polyethylene glycols.

For most proteins, suitable crystallization conditions require a specific combination of these parameters. Often changes as small as 0.1 pH unit can affect the quality of, or even the ability to grow protein crystals. In spite of this, these trial-and-error techniques have permitted a number of proteins to be crystallized during the past few years. However, there is a growing list of important proteins that have not yet been crystallized despite intensive efforts. Some proteins merely form amorphous precipitates that display no evidence of crystallinity. This is not surprising, since proteins have a large number of sites capable of intermolecular interactions but relatively few which will produce the precise alignment of molecules necessary for crystal formation. In other cases, small

microcrystals may be obtained readily, but these crystals cannot be induced to grow large enough for structural studies. Most researchers agree that protein purity and homogeneity are usually necessary for crystallization efforts to be successful. It has been suggested that the presence of impurities may prevent crystallization or terminate crystal growth prematurely after nucleation. There are also numerous examples of proteins that produce relatively large crystals which display such severe internal disorder that high-resolution structural analyses are not possible.

Physical factors such as convective flow effects (Fig. 2) may also influence crystal growth.

Clearly there is a need for basic studies of both the nucleation and growth phases of protein crystals. Without a fundamental knowledge of these processes, crystallographers will be forced to continue to rely on time consuming, trial-and-error methods of the past.

Recent advances in protein crystal growth

Although protein crystal growth continues to be a major bottleneck in widespread applications of protein crystallography, several promising new approaches are emerging.

Surfactants

One of the most exciting developments is the progress that has been made in crystallization of membrane proteins. Three-dimensional crystals of integral membrane proteins of sufficient quality to produce X-ray diffraction patterns were first reported for bacteriorhodopsin, isolated from the purple membrane of halobacteria[9], for porin, an outer membrane protein from *Escherichia coli*[10], and more recently for the photoreaction center from *Rhodopseudomonas viridis*[11,12]. Crystallization of these membrane proteins was achieved using short chain surfactants (detergents) which are believed to shield the hydrophobic intramembranous surfaces of the molecules thereby allowing polar interactions between molecules to be the stabilizing force in the crystals. In some cases, the quality of the crystals (as evidenced by both appearance and resolution limits of the X-ray diffraction patterns) could be improved using small amphiphilic molecules such as heptane 1,2,3-triol[13–15] mixed with surfactants. The strategy is to optimize contacts between the protein-surfactant micelles by altering the size and/or ionic characteristics of the micelle. It has been hypothesized that the small amphiphilic molecules act by forming mixed micelles with surfactants, which are smaller than the pure surfactant micelles. To date, several membrane proteins have been crystallized with some yielding crystals of sufficient quality for high-resolution crystallographic analysis[11,13,15–20]. Experience with new synthetic detergents and amphiphilic molecules will most probably increase the chances of obtaining useful crystals of many other membrane proteins. It has been found that detergents such as β-octylglucoside are also useful for crystallization experiments with hydrophilic proteins[21], possibly by interfering with nonspecific interactions that compete with those that are favorable for crystal growth.

Fig. 2

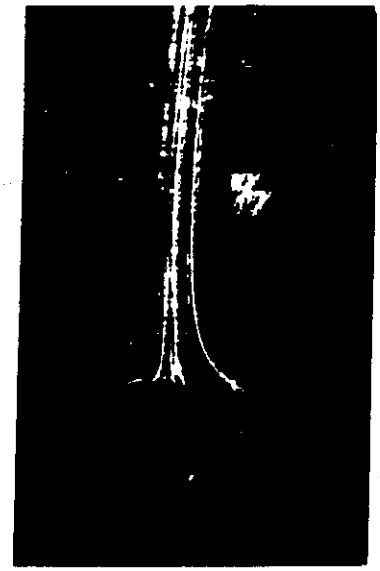

Gravitational effects on crystal: convective flow effects. A Schlieren photograph of a triglycine crystal growing under unit gravity at isothermal conditions. Schlieren photography highlights differences in refractive index; the lighter regions show the parts of the solution which have lower density. As material is incorporated onto the surface of the growing crystal, density variations occur in the surrounding solution. Under gravitational influence, the low density solution around the crystal rises thereby producing convective flow patterns. The turbulence created by this flow may influence crystal growth by creating non-uniform conditions across the crystal surface, by forcing the solution to flow at such a rate that steady-state diffusion ceases to be a rate-limiting step in growth, and by generating convective stirring effects which can cause multiple nucleation sites within the solution. The crystal here is approximately 1.5 × 0.4 cm and is attached to a glass rod which is vertical in the photograph. (Kindly provided by Roger Kroes and William Witherow.)

Mechanisms

Especially encouraging progress is now being made in experimental and theoretical studies of the principles of protein crystal growth. Investigations regarding the mechanisms of protein crystal nucleation, growth and growth cessation have recently been reported[8,22–25] and have indicated that optimum protein crystal growth requires much more careful monitoring and control of major parameters (i.e. rate of protein concentration, temperature etc.) than is possible with current techniques. Generally, it has been observed that larger and better crystals are obtained if the rate of equilibrium is decreased. A prototype vapor diffusion system that permits dynamic control of equilibration rates during protein crystal growth processes has been developed recently[26], and efforts to automate this system are in progress.

Robotics has also been applied to protein crystal growth experiments[27–29]. Several systems have been developed to automate present techniques for hanging drop (vapor diffusion) experiments. Automated syringes inject and mix protein precipitant solutions on the glass coverslip. Reservoir solutions are then automatically injected into a depression or well onto which the inverted coverslip is placed.

Dynamic light-scattering methods have been used to monitor nuclea-

Fig. 3

Payload specialist, Congressman Bill Nelson, performing protein crystal growth experiments in space on STS-61C.

tion events during protein crystal growth, thus permitting nucleation and growth to be separated and controlled as different processes[30,31]. Quasi-elastic light scattering can be used to monitor the effects of protein concentration on the size and shape distribution of small aggregates in protein solutions, and efforts to apply this information for controlling crystal formation are in progress. The considerable body of theoretical and experimental data relating to the growth of organic and inorganic crystals is now being applied to protein crystal growth. It is likely that the multi-disciplinary fundamental protein crystal growth studies now in progress will lead to a much better understanding of the basic processes involved, and will result in much more powerful experimental systems for dynamically monitoring and controlling protein crystal growth.

Space experiments

One promising new development in protein crystal growth involves studies of crystal growth in the microgravity environment obtainable in space (Fig. 3). Crystal growth has been of considerable interest to the National Aeronautics and Space Administration (NASA) and to other space-oriented researchers for a number of years[32], and several fundamental studies of crystal growth in space are in progress. The major motivation behind these space experiments is to examine the effects that density-driven convective flow has on crystal growth. Under microgravity conditions, convective flow patterns (Fig. 2) are suppressed. The absence of gravity therefore provides a direct way to examine the role of convection on crystal growth. In addition, microgravity conditions may serve to minimize sedimentation, which can interfere with uniform growth of protein crystals (Fig. 4a). Since protein crystals are extremely fragile, one might expect that protein crystal formation would be particularly affected by fluctuations in the growth environment, including those caused by gravitational effects.

Several laboratories around the world are involved in efforts to investigate gravitational effects on protein crystal growth. The first reported space experiments[33] involved the growth of lysozyme and β-galactosidase crystals on Spacelab I. These preliminary studies indicated that the space-grown protein crystals are larger than crystals of these proteins obtained under the same experimental conditions on earth.

Subsequent space experiments, coordinated through NASA's Marshall Space Flight Center in Huntsville, Alabama, have involved prototype hardware development, and protein crystal growth on four different shuttle flights in 1985 and 1986[34]. The latest hardware version which was flown in January 1986 on shuttle flight STS-61C (Fig. 5) consists of twenty-four vapor-diffusion chambers, with syringe mechanisms for activating and deactivating the experiments. Once in orbit, the

Fig. 4

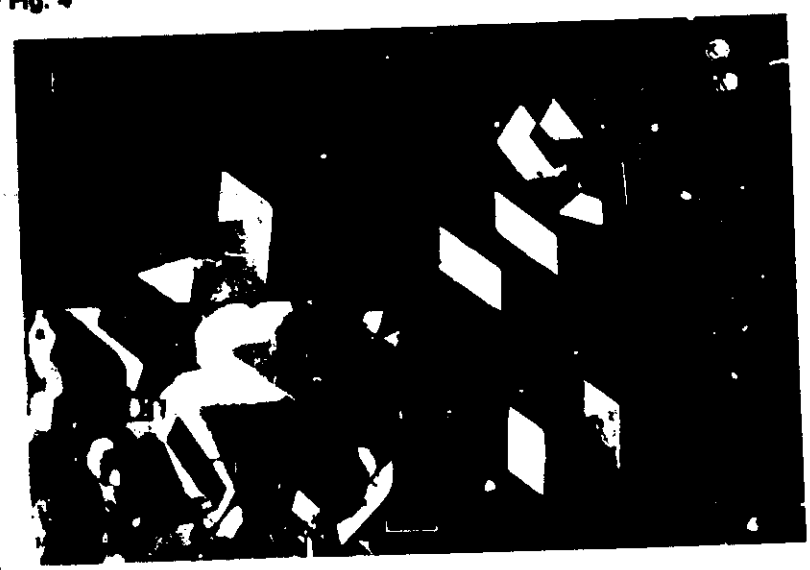

Crystals of canavalin: (a) grown in flight hardware under controlled conditions on earth: (b) grown under microgravity conditions on shuttle flight STS-61C.

Fig. 5

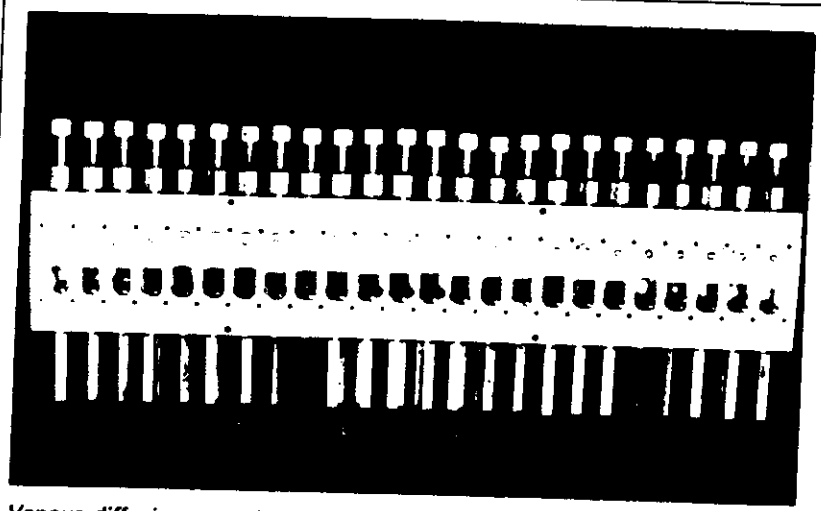

Vapour diffusion crystal growth hardware. One complete unit consists of twenty-four syringes and plungers. Bar, 5 cm.

experiments are activated by extruding protein solutions from the syringes forming droplets on the syringe tips. These droplets are then permitted to equilibrate with reservoir solutions in the chambers.

The resulting crystals of canavalin growing in 40 μl droplets are shown in Fig. 6. The NASA protein crystal growth project is in the initial stages, and the space experiments have been primarily used to develop reliable vapor-diffusion techniques that may be used in the future for systematically evaluating gravitational effects on protein crystal growth. The prototype system (Fig. 5) evolved over the course of the four shuttle flight experiments, and the current version of the hardware worked well on the last mission, producing crystals of all proteins that were included (hen egg white lysozyme, human serum albumin, human C-reactive protein, bacterial purine nucleoside phosphorylase, canavalin, and concanavalin B).

It is clear that microgravity conditions can have remarkable effects on crystal morphology in some cases, as evidenced particularly by the crystal growth studies with canavalin. Canavalin crystals grown in hanging droplets on earth quickly sediment to the bottom of the droplets and grow as fused aggregates of poorly formed crystals (Fig. 4a). Under microgravity conditions, canavalin crystals grow dispersed through the droplets (Fig. 5) resulting in uniform morphologies for nearly all of the canavalin crystals (Fig. 4b). Interesting morphology changes were also noted for crystals of human C-reactive protein and for human serum albumin.

Detailed studies of microgravity effects on protein crystal growth must await future shuttle flights. The prototype hardware that has been developed will form the basis for the design of automated systems that permit dynamic monitoring and control of key variables including temperature, protein concentration, ionic strength, pH, and precipitating agent concentration. This hardware should prove useful for both ground-based and space experiments that are directed at better understanding of protein crystal growth processes.

Fig. 6

Canavalin crystals growing in a 40 μl droplet under microgravity conditions. Bar, 1 mm.

Conclusions

It has become clear that the exciting applications of protein crystallography cannot be utilized to their full potential until the basic principles of protein crystal growth are better understood and new experimental techniques for crystallizing proteins are developed. This recent effort, already rewarded by success, is likely to continue to develop rapidly during the next few years.

Acknowledgement

Portions of this work were supported by NASA grant No. NAGW-813 and NASA contract No. NAS8-36611.

References

1 Kendrew, J. C., Dickerson, R. E., Strandberg, B. E., Hart, R. G., Davies, D. R., Phillips, D. C. and Shore, V. C. (1960) *Nature* 185, 442–427
2 Blundell, T. L. and Johnson, L. M. (1976) *Protein Crystallography* Academic Press, New York
3 Kossiakoff, A. A. (1985) *Ann. Rev. Biochem.* 54, 1195–1227
4 McPherson, A. (1982) *Preparation and Analysis of Proteins Crystals* John Wiley & Sons
5 Giege, R., Dock, A. C., Kern, D., Lorber, B., Thierry, J. C. and Moras, D. (1986) *J. Crystal Growth* 76, 554–561
6 Zeppezauer, M., Eklund, H. and Zeppezauer, E. (1968) *Arch. Biochem. Biophys.* 126, 564–573
7 Salemme, F. R. (1972) *Arch. Biochem. Biophys.* 151, 533–539
8 Solemme, F. R. *Methods in Enzymology* (1985) 114, 140–141
9 Michel, H. and Oesterhelt, D. (1980) *Proc. Natl Acad. Sci USA* 77, 1283–1285
10 Garavito, R. M. and Rosenbusch, J. P. (1980) *J. Cell Biol.* 86, 327–329
11 Deisenhofer, J., Epp, O., Miki, L.,

Huber, R. and Michel, H. (1984) *J. Mol. Biol.* 180, 385–398
12 Deisenhofer, J., Epp, O., Miki, K., Huber, R. and Michel, H. (1985) *Nature* 318, 618–623
13 Michel, H. (1982) *J. Mol. Biol.* 158, 567–572
14 Michel, H. (1983) *Trends Biochem. Sci.* 8, 56–59
15 Michel, H. (1982) *EMBO J.* 1, 1267–1271
16 Garavito, R. M., Jenkins, J. A., Jansonius, J. N., Karlsson, R. and Rosenbusch, J. P. (1983) *J. Mol. Biol.* 164, 313–327
17 Garavito, R. M., Hinz, U. and Neuhaus, J. M. (1984) *J. Biol. Chem.* 259, 4254–4257
18 Allen, J. P. and Feher, G. (1984) *Proc. Natl Acad. Sci. USA* 81, 4795–4799
19 Welte, W., Wacker, T., Leis, M., Kreutz, W., Shinozawa, J., Gad'on, N. and Drews, G. (1985) *FEBS Lett.* 182, 260–264
20 Chang, C-H., Schiffer, M., Tiede, D., Smith, U. and Norris, J. (1985) *J. Mol. Biol.* 186, 201–203
21 McPherson, A., Koszelak, S., Axelrod, H., Day, J., Williams, R., Robinson, L., McGrath, M. and Cascid, D. (1986) *J. Biol. Chem.* 261, 1969–1975
22 Fiddis, R. W., Longman, R. A. and Calvert, P. D. (1979) *Trans. Faraday Soc.* 75, 2753–2757
23 Kam, Z., Shore, H. B. and Feher, G. (1978) *J. Mol. Biol.* 123, 539–555
24 Pusey, M. L., Snyder, R. S. and Naumann, R. (1986) *J. Biol. Chem.* 261, 6524–6529
25 Rosenberger, F. (1986) *J. Crystal Growth* 76, 618–638
26 Suddath, F. L., Wilson, L. J. and Bertrand, J. (1987) *Dynamic Control of Protein Crystallization*, American Crystallographic Association Meeting, March 15–20, Austin, Texas, Abst. H–2
27 Jones, N. D., Decter, J. B., Swartzenderber, J. K. and Landis, P. L. (1987) *Apocalypse – An Automated Protein Crystallization System*, American Crystallographic Association Meeting, March 15–20, Austin, Texas, Abst. H–4
28 Ward, K. B., Perozzo, M. A. and Zuk, W. M. (1987) *Automated Preparation of Protein Crystals Using Laboratory Robotics and Automated Visual Inspection*, American Crystallographic Association Meeting, March 15–20, Austin, Texas, Abst. H–3
29 Weber, P. C. and Cox, M. J. (1987) *Experiments with Automated Protein Crystal Growth*, American Crystallographic Association Meeting, March 15–20, Austin, Texas, Abst H–5
30 Carter, C. W., Jr and Carter, C. W. (1979) *J. Biol. Chem.* 254, 12219–12223
31 Baldwin, E. T., Crumley, K. V. and Carter, C. W., Jr (1986) *Biophys. J.* 49, 47–48
32 Rindone, G. E., ed. (1982) *Materials Processing in the Reduced Gravity Environment of Space*, North–Holland
33 Littke, W. and John, C. (1984) *Science* 225, 203–204
34 DeLucas, L. J., Suddath, F. L., Snyder, R., Naumann, R., Broom, M. B., Pusey, M., Yost, V., Herren, B., Carter, D., Nelson, B., Meehan, E. J., McPherson, A. and Bugg, C. E. (1986) *J. Crystal Growth* 76, 681–693

Protein Crystal Growth in Microgravity

LAWRENCE J. DELUCAS, CRAIG D. SMITH, H. WILSON SMITH, SENADHI VIJAY-KUMAR, SHOBHA E. SENADHI, STEVEN E. EALICK, DANIEL C. CARTER, ROBERT S. SNYDER, PATRICIA C. WEBER, F. RAYMOND SALEMME, D. H. OHLENDORF, H. M. EINSPAHR, L. L. CLANCY, MANUEL A. NAVIA, BRIAN M. MCKEEVER, T. L. NAGABHUSHAN, GEORGE NELSON, A. MCPHERSON, S. KOSZELAK, G. TAYLOR, D. STAMMERS, K. POWELL, G. DARBY, CHARLES E. BUGG

The crystals of most proteins or other biological macromolecules are poorly ordered and diffract to lower resolutions than those observed for most crystals of simple organic and inorganic compounds. Crystallization in the microgravity environment of space may improve crystal quality by eliminating convection effects near growing crystal surfaces. A series of 11 different protein crystal growth experiments was performed on U.S. space shuttle flight STS-26 in September 1988. The microgravity-grown crystals of γ-interferon D[1], porcine elastase, and isocitrate lyase are larger, display more uniform morphologies, and yield diffraction data to significantly higher resolutions than the best crystals of these proteins grown on Earth.

PROTEIN CRYSTALLOGRAPHY REquires crystals of suitable size and quality for high-resolution diffraction analyses. A new development in protein crystal growth involves studies of crystal growth processes in the microgravity environment obtainable in space (*1, 2*). The major motivation behind these space experiments is to eliminate the density-driven convective flow that accompanies crystal growth in gravitational fields (*3, 4*). In addition, sedimentation of growing crystals, which can interfere with the formation of single crystals, is eliminated in the absence of gravity.

Microgravity protein crystal growth experiments performed on Spacelab 1 by Littke and John (*5*) indicated that the space-grown crystals from a liquid-liquid diffusion system were larger than crystals obtained by the same experimental system on Earth. Experiments on four U.S. space shuttle missions in 1985 and 1986 led to development of an apparatus for protein crystal growth by vapor diffusion techniques (*6*). We used this equipment for a series of protein crystal growth experiments on U.S. space shuttle flight STS-26 in September 1988. The results of these experiments are presented.

The vapor diffusion technique used on STS-26 is closely related to the hanging drop method (*7*), and thus the microgravity results can be compared with extensive data obtained from experiments on Earth. The hardware was adapted from that used on a series of four shuttle missions in 1985 and 1986 (*6*). Crystals were grown in 40-μl droplets that were extruded from syringes and subsequently permitted to equilibrate with solutions of precipitating agents contained within closed chambers. Each experiment was performed within a chamber (5.3 cm^3) with clear plastic windows. Before the launch, a double-barreled syringe was loaded with protein solution and crystallizing (precipitating) solutions in adjacent barrels. The mouths of these double-barreled syringes were stoppered during launch and landing. The chamber contained an absorbent material that was saturated with a solution of the precipitating agent. All solutions were loaded ~24 hours before the launch. Once in orbit, crystal growth was activated by extruding the solutions onto the tip of the syringe, where mixing of the protein solution and precipitating agent was achieved by repeatedly withdrawing and extruding the solutions. The suspended droplet was then allowed to equilibrate with the surrounding solution of precipitating agent. The protein droplets were photographed after activation and at 24-hour intervals during the 3-day experiments. After 3 days, the solutions and suspended crystals were withdrawn into the syringes and stoppered for return to Earth (*8*).

Control experiments on Earth were performed in equipment identical to that used for the shuttle experiments. The control experiments were begun 7 days after the shuttle landed; the same protein solutions and identical loading, activation, and deactivation times were used in the control experiments as in the STS-26 experiments. Extensive control experiments were also performed in prototypes of the space shuttle hardware before and after the shuttle experiments were completed.

X-ray diffraction photographs were used for qualitative evaluation of diffraction resolutions. The results from these analyses are consistent with the more detailed studies of three-dimensional (3-D) data sets measured with the area detector systems (*9*). Because evaluation of diffraction resolutions from photographs is highly subjective, and is often dependent on crystal orientations, we have depended primarily on 3-D intensity data sets for comparison of space- and Earth-grown crystals.

Intensity data sets from crystals of three proteins were analyzed in a variety of different ways (Fig. 1). The largest Bragg angles at which usable data could be measured were assembled, and the percentage of data above background levels throughout the data collection range was evaluated. Plots were made of average $I/\sigma(I)$ values, where I is intensity, versus diffraction resolution and of percentages of data above various cutoff levels as functions of resolution. Data sets from space- and Earth-grown crystals were compared by using Wilson plots (*10*). The Wilson plot can be used to estimate the

L. J. DeLucas, C. D. Smith, H. W. Smith, S. Vijay-Kumar, S. E. Senadhi, S. E. Ealick, C. E. Bugg, University of Alabama at Birmingham, Center for Macromolecular Crystallography, Birmingham, AL 35294.
D. C. Carter and R. S. Snyder, George Marshall Space Flight Center, Huntsville, AL 35812.
P. C. Weber, F. R. Salemme, D. H. Ohlendorf, E. I. du Pont de Nemours & Company, Central Research and Development Department, Wilmington, DE 19880.
H. M. Einspahr and L. L. Clancy, Upjohn Company, Kalamazoo, MI 49001.
M. A. Navia and B. M. McKeever, Merck Sharp & Dohme Research Laboratories, Rahway, NJ 07065.
T. L. Nagabhushan, Schering-Plough Corporation, Bloomfield, NJ 07003.
G. Nelson, Astronomy Department, University of Washington, Seattle, WA 98195.
A. McPherson and S. Koszelak, University of California at Riverside, Riverside, CA 92521.
G. Taylor, Laboratory of Molecular Biophysics, University of Oxford, Oxford OX1 3QU, United Kingdom.
D. Stammers, K. Powell, G. Darby, Wellcome Research Laboratories, Beckenham BR3 3BS, United Kingdom.

overall B values for a crystal, the B value being a parameter that reflects the internal order within a crystal. Relative Wilson plots, also known as difference Wilson plots (*10*), are useful for assessing changes in the internal order of protein crystals. These plots of $\ln(\Sigma F_a^2/\Sigma F_b^2)$, where F is the crystallographic structure factor for crystals of type a and b, versus 4 $\sin^2 \theta/\lambda^2$ (resolution) are routinely used to characterize and compensate for the disordering effects resulting from the diffusion of heavy-atom derivatives into protein crystals. The slopes of these plots are directly related to the difference in overall B values for two different crystals, a (Earth-grown) and b (space-grown).

The STS-26 experiments included an engineered native form of γ-interferon D^1 (γ-IFN D^1). Crystals of γ-IFN D^1 are trigonal (space group $R32$, with $a = b = 114$ Å and $c = 315$ Å). The crystals were grown from a solution of 49% ammonium sulfate, 0.05M sodium acetate, pH = 5.9 (*11*). Many crystallization experiments were performed at the University of Alabama at Birmingham with this protein over a 2-year period, and 3-D intensity data sets were collected. For STS-26, five crystallization experiments were performed under conditions identical, except for gravity, to those routinely used for crystal growth studies on Earth. Two crystals were obtained that were larger than the best that have been produced in any ground experiments; one was ~50% larger than the largest crystal that had been obtained previously. The overall morphology was similar to the Earth-grown crystals.

The 3-D intensity data for the STS-26 crystal were compared with data sets obtained from four Earth-grown crystals. The space-grown crystal displayed an increase in measurable data throughout the resolution range, with a significant fraction of measured data beyond 3.0 Å resolution, where the Earth-grown crystals displayed no significant diffraction.

Although this improvement could reflect enhanced counting statistics resulting from the larger crystal volume, examination of a relative Wilson plot indicated that the space-grown crystal has a lower effective B value. This relative Wilson plot is shown in Fig. 2A, where the data from the space-grown crystal is scaled to the data from an Earth-grown crystal. If the B values of the two crystals were comparable, the relative Wilson plot should be flat with a slope of zero. For comparative purposes, a Wilson plot based on data from two of the Earth-grown γ-IFN D^1 crystals is shown. The slope for this plot is essentially zero, whereas the space versus ground plot displays a positive slope throughout the resolution range, with a steeper slope at the higher resolutions, indicating that the B value for the space-grown crystal is lower than that for the Earth-grown crystal.

Crystals of porcine elastase are orthorhombic (space group $P2_12_12_1$, with a = 50.9 Å, b = 57.2 Å, and c = 75.0 Å). Crystals were grown by seeding techniques from solutions of precipitant (1.5M sodium sulfate, 0.1M sodium acetate, pH = 5.0) (*12*). Small seed crystals were added to the solution of precipitating agent in one side of the double-barreled syringes. The seed crystals used were ~50 μm in the maximum dimension. A number of well-formed elastase crystals in the range of 0.5 to 2.1 mm were obtained from six crystallization experiments on STS-26. Comparison of 3-D intensity data for a space-grown crystal with dimensions comparable to Earth-grown crystals studied earlier (*13*) (Fig. 1B) revealed that the space-grown crystal yielded significantly more data at all resolution ranges, with enhancement in the ultimate resolution at which measurable data can be obtained. The relative Wilson plot (Fig. 2) did not reveal a significant difference in B values for data in the lower resolution ranges, but the higher resolution data indicated that the space-grown crystal had a significantly lower overall effective B value.

Crystals of isocitrate lyase are orthorhombic (space group $P2_12_12_1$, with a = 80.7 Å, b = 123.1 Å, and c = 183.4 Å). Crystals are grown from a solution of 1.7M sodium citrate, 0.1M tris-HCl, pH = 8.0. Crystallization experiments (*14*) have invariably resulted in the growth of dendritic clusters (Fig. 3A).

An improved habit for isocitrate lyase was observed from the experiments on STS-26. Although some dendritic growth was found in the space samples, a number of well-

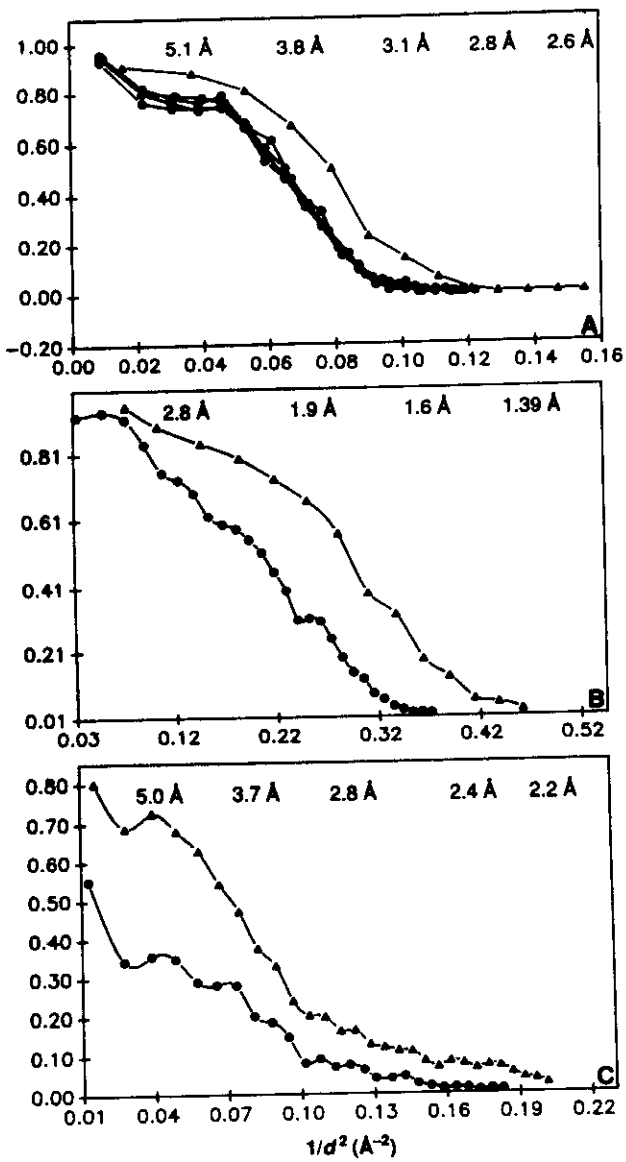

Fig. 1. Comparison of diffraction intensity data for space-grown (▲) and Earth-grown (●) crystals of (A) γ-IFN D^1, (B) porcine elastase, and (C) isocitrate lyase. The y axis shows the fraction of data with $I/\gamma(I) \geq 5$. (**A**) Space-grown γ-IFN D^1 crystal and the data obtained from four of the largest Earth-grown crystals of γ-IFN D^1. (**B**) Space-grown porcine elastase crystal and a porcine elastase crystal of comparable size grown on Earth. (**C**) Comparison of intensity distributions for space-grown and Earth-grown crystals of isocitrate lyase.

These prisms belong to the same space group as the Earth-grown dendrites, but they yielded better intensity data throughout the intensity range (Fig. 1C). A relative Wilson plot (Fig. 2C) indicated that, except at the lowest resolution range, the space-grown crystal had a significantly lower effective B value than the Earth-grown crystal.

Of the eight other proteins crystallized on STS-26 (*15*), six did not produce crystals large enough for diffraction analysis. One produced only a partial data set, the analysis of which was inconclusive when compared to Earth data. The final protein (canavalin) displayed higher resolution (~0.2 Å) on the film data, but the 3-D data could not be processed because of experimental difficulties that arose during the data collection process.

The improved diffraction patterns from the space-grown crystals may not be entirely attributable to enhanced internal order of the crystals. Intensity data sets were collected in three different laboratories in order to obtain the data as rapidly as possible after the space experiments and to collect data at locations where Earth-grown crystals were routinely analyzed. Although the same type of area detector system was used in these three laboratories, there were variations in data collection procedures. However, when the results for these experiments are considered together, the data indicate that protein crystals grown under microgravity conditions diffract to higher resolution than the best crystals obtained under similar conditions on Earth. The lack of success for six of the eight remaining proteins is attributed to nonoptimum crystal growth conditions for the space experiment.

The relative Wilson plots indicate that the space-grown crystals are more highly ordered at the molecular level than crystals grown by the same method on Earth. Under microgravity conditions, convective flow patterns that accompany crystal growth would be eliminated, thus generating a more controlled environment at crystal interfaces. Because protein crystals are relatively weakly bonded, with water bridges playing predominant roles, molecular-packing patterns may be more regular in the absence of convective turbulence. The ability to grow protein crystals with increased molecular order should enhance crystallographic solutions by shortening the time required to determine the structure and by increasing the accuracy of molecular details.

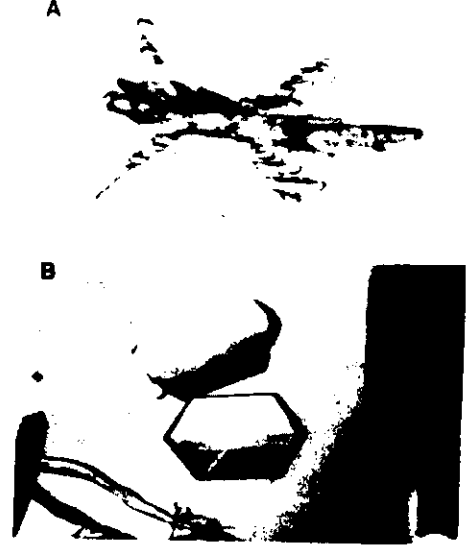

Fig. 3. (**A**) Typical dendritic morphology for isocitrate lyase crystals grown on Earth. The dimensions of this dendritic cluster are 0.74 and 0.46 mm, respectively. (**B**) Prisms of isocitrate lyase grown on STS-26. The crystal dimensions are approximately 0.4 mm by 0.25 mm by 0.4 mm.

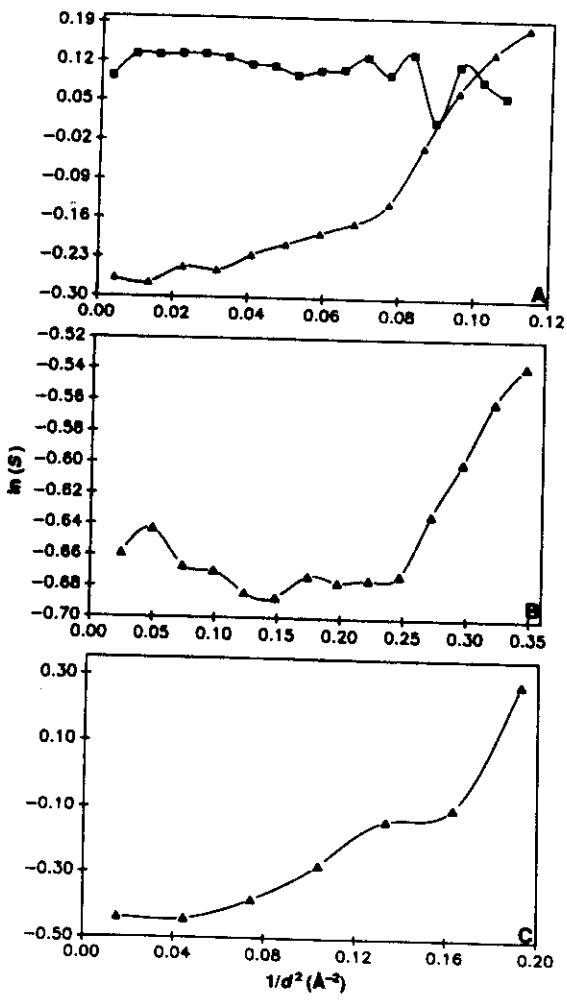

Fig. 2. Relative Wilson plot (▲) comparing space-grown and Earth-grown crystals of (**A**) γ-IFN D¹, (**B**) porcine elastase, and (**C**) isocitrate lyase. In addition, a relative Wilson plot (■) comparing two Earth-grown crystals of γ-IFN D¹ is shown in (A). $S = \Sigma F_a^2/\Sigma F_b^2$.

REFERENCES AND NOTES

1. L. J. DeLucas and C. E. Bugg, *Trends Biotechnol.* 76, 188 (1987).
2. C. E. Bugg, *J. Cryst. Growth* 76, 535 (1986).
3. M. Pusey, W. Witherow, R. Naumann, *ibid.* 90, 105 (1988).
4. R. L. Kroes and D. Reiss, *ibid.* 69, 414 (1984).
5. W. Littke and C. John, *Science* 225, 203 (1984).
6. L. J. DeLucas *et al.*, *J. Cryst. Growth* 76, 681 (1986).
7. A. McPherson, *Methods Enzymol.* 114, 112 (1985).
8. The experimental apparatus was contained within a temperature-controlled module that was maintained at 22.8° ± 0.7°C from the time that the samples were loaded until the analyses of the crystals could be performed. Slightly higher temperatures occurred for short periods of time during the photographic sessions. Immediately after the shuttle landed, the hardware was transported in the incubator to Birmingham, Alabama, where the analyses were initiated. The space-grown crystals were extruded into depression plates, sealed with glass cover slips, and photographed with the use of a binocular microscope. Selected crystals were sealed in glass capillaries for x-ray diffraction analysis.
9. X-ray diffraction photographs were obtained with crystals in stationary orientations by the use of specially constructed cylindrical cassettes mounted on rotating anode x-ray generators. More detailed x-ray diffraction studies were performed with Nicolet area detector systems [A. J. Howard *et al.*, *J. Appl. Crystallogr.* 20, 383 (1987)] mounted on rotating anode x-ray generators with copper targets, at the University of Alabama at Birmingham (for γ-IFN D¹ and canavalin), du Pont (for isocitrate lyase), Merck (for porcine elastase), and the Marshall Space Flight Center (for human serum albumin).
10. T. L. Blundell and L. N. Johnson, *Protein Crystallography* (Academic Press, New York, 1976), pp. 333–336.
11. S. Vijay-Kumar *et al.*, *J. Biol. Chem.* 262, 4804

(1987).
12. L. Sawyer *et al.*, *J. Mol. Biol.* **18**, 137 (1978).
13. M. A. Navia and B. M. McKeever, unpublished data.
14. P. C. Weber, F. R. Salemme, D. H. Ohlendorf, unpublished data.
15. Canavalin, human serum albumin, human C-reactive protein, snake venom phospholipase A_2, human renin, synthetic peptide, human purine nucleoside phosphorylase, and human immunodeficiency virus reverse transcriptase.

16. Supported by NASA contract NAS8-36611 and NASA grant NAGW-813. We thank D. Jex, R. Naumann, members of Teledyne-Brown Engineering Company who designed and constructed our protein crystal growth apparatus, the many NASA employees who helped at all stages of the shuttle activities, and F. Suddath for invaluable assistance in developing a space version of the hanging drop method.

25 May 1989; accepted 29 August 1989

Proc. Natl. Acad. Sci. USA
Vol. 88, pp. 11540–11544, December 1991
Biophysics

Application of crystallographic and modeling methods in the design of purine nucleoside phosphorylase inhibitors

STEVEN E. EALICK*, Y. SUDHAKAR BABU†, CHARLES E. BUGG*†, MARK D. ERION‡, WAYNE C. GUIDA‡, JOHN A. MONTGOMERY†§, AND JOHN A. SECRIST III§

*University of Alabama, Birmingham, AL 35294; †BioCryst, Inc., Birmingham, AL 35205; ‡CIBA-Geigy Corp., Summit, NJ 07901; and §Southern Research Institute, Birmingham, AL 35255-5305

Communicated by Brian W. Matthews, July 8, 1991 (received for review February 6, 1991)

ABSTRACT **Competitive inhibitors of the salvage pathway enzyme purine-nucleoside phosphorylase (purine-nucleoside:orthophosphate ribosyltransferase, EC 2.4.2.1) have been designed by using the three-dimensional structure of the enzyme as determined by x-ray crystallography. The process was an iterative one that utilized interactive computer graphics, Monte Carlo-based conformational searching, energy minimization, and x-ray crystallography. The proposed compounds were synthesized and tested by an *in vitro* assay. Among the compounds designed and synthesized are the most potent competitive inhibitors of purine nucleoside phosphorylase thus far reported.**

The concept of drug design based on crystallographic and modeling methods has received much attention, yet few solid examples have appeared in the literature. Two notable exceptions are the reports by Erickson *et al.* (1) on the design of human immunodeficiency virus protease inhibitors and Appelt *et al.* (29) on the design of thymidylate synthase inhibitors. Advances in crystallography, computer graphics, and related fields have resulted in a dramatic increase in the number of macromolecular structure determinations while advances in computer hardware and computational methods have allowed the computational chemist to address more complex problems with higher accuracy (2, 3). Clearly, structural information combined with graphical methods for depicting the accessible volume, electrostatic potential, and active-site hydrophobicity aids drug design. Further enhancement in the quality of the "designed compounds" is expected from methods that can accurately evaluate the target molecule in terms of binding conformation, binding affinity, and binding-induced changes in protein conformation. We have developed Monte Carlo-based conformational search methods that, in combination with energy minimization, accurately predict the crystallographically observed ligand binding conformations for enzyme–inhibitor complexes. We now report the use of crystallographic and modeling methods for the design of competitive inhibitors of the enzyme purine nucleoside phosphorylase (PNP; purine nucleoside:orthophosphate ribosyltransferase, EC 2.4.2.1).¶

PNP as a Target for Drug Design. PNP catalyzes the reversible phosphorolysis of purine ribo- or 2′-deoxyribonucleosides to the purine and ribose- or 2-deoxyribose-α-1-phosphate. The enzyme has been isolated from both eukaryotic and prokaryotic organisms (4) and functions in the purine salvage pathway (5, 6). PNP isolated from human erythrocytes is specific for the 6-oxypurines and many of their analogs (7), while PNPs from other organisms vary in their specificity (8). The human enzyme is a trimer with identical subunits and a total molecular mass of ≈97 kDa (9, 10).

Interest in PNP as a drug target arises from its ability to rapidly metabolize purine nucleosides and from its role in the T-cell branch of the immune system. The chemotherapeutic potential of purine nucleoside analogs such as the 6-thiopurine 2′-deoxyribonucleosides (11) and 2′,3′-dideoxyinosine (12) may be severely compromised by PNP metabolism. Hence, a combination of a PNP inhibitor with these compounds may be highly efficacious. Administered alone, PNP inhibitors have potential therapeutic value since children lacking PNP activity exhibit severe T-cell immunodeficiency while maintaining normal B-cell function (13). This profile suggests utility for PNP inhibitors in the treatment of T-cell leukemias or lymphomas, in organ transplantation, and in T-cell-mediated autoimmune diseases such as rheumatoid arthritis and lupus. Despite the potential benefits of PNP inhibitors and despite the large number of PNP inhibitors that have been synthesized to date (4, 14), no compound has yet reached clinical trials. Although potencies for the best compounds have affinities 10–100 times higher than the natural substrate (K_m, ≈40 μM), it is expected that T-cell immunotoxicity will require very tight binding inhibitors (K_i, <10 nM) due to the high *in vivo* PNP activity and competition with substrate (15). Hence, we determined the structure of human PNP (Fig. 1) by x-ray crystallography (16) and have used these results in combination with computer-assisted molecular modeling to design highly potent inhibitors of this key enzyme.

Overall Strategy for Inhibitor Design. Once the structure of PNP was known, a scheme was used that involved both inhibition data and x-ray crystallography for evaluation of the synthesized compounds and a combination of these data and molecular modeling for the design of the next round of target molecules. A flow chart describing the overall strategy is shown in Fig. 2. Proposed compounds were screened by modeling the enzyme–inhibitor complex by using interactive computer graphics (17) and AMBER (18, 19) based molecular energetics. Monte Carlo/energy minimization techniques (20) were used to sample the conformational space available to potential inhibitors docked into the PNP active site. Qualitative evaluation of the enzyme–inhibitor complexes by molecular graphics and semiquantitative evaluation of the interaction energies between the inhibitors and the enzyme aided in prioritization for chemical synthesis. The resulting compounds were evaluated by determination of their IC_{50} values and by x-ray diffraction analysis using difference Fourier maps. The details of the modeling studies, organic syntheses, and x-ray diffraction experiments will be published elsewhere. The results of these analyses frequently led to proposed modifications of existing compounds or to the identification of new target compounds. Further analyses,

The publication costs of this article were defrayed in part by page charge payment. This article must therefore be hereby marked "*advertisement*" in accordance with 18 U.S.C. §1734 solely to indicate this fact.

Abbreviation: PNP, purine nucleoside phosphorylase.

¶The atomic coordinates and structure factors for PNP and PNP–guanine complex have been deposited in the Protein Data Bank, Chemistry Department, Brookhaven National Laboratory, Upton, NY 11973 (reference PNP3, PNP4) and will be released 1 year from the date of publication.

FIG. 1. Three-dimensional structure of human PNP. Each subunit in the trimer is represented by a ribbon that passes through the α-carbon positions. The molecule is viewed down the trimer axis. The ribbon is color-coded by secondary structure such that β-strands are green, α-helices are blue, and loops and turns are white. The substrates guanosine and phosphate are shown in the active site as ball and stick models.

such as K_i determinations and *in vivo* assays, were performed on the most potent compounds. Using this iterative process we were able to improve the potency of the best known membrane-permeable competitive PNP inhibitors by almost 2 orders of magnitude.

Description of the Active Site of PNP. The PNP trimer possesses three identical active sites near the interface between adjacent subunits. Each individual active site utilizes residues primarily from one subunit; however, participation of Phe-159 in the adjacent subunit is observed. The arrangement of key amino acids in the active site of PNP is shown in Fig. 3. The purine binding site is the most deeply buried and specificity for analogs of the 6-oxypurines is provided by Glu-201 and Lys-244, which form hydrogen bonds with purine atoms N(1)-H and O(6). The remainder of the purine binding site is largely hydrophobic, being composed of residues Ala-116, Phe-200, Val-217, Met-219, and Phe-159 of another subunit. These residues along with Thr-242 and Asn-243 form a cavity that accommodates a purine base.

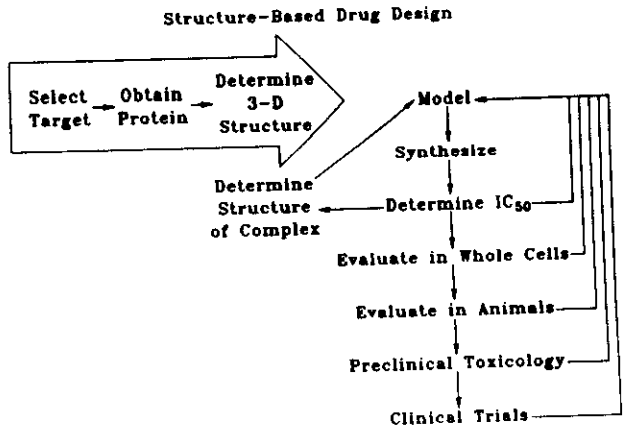

FIG. 2. Flowchart showing the overall strategy for the design of competitive inhibitors of purine nucleoside phosphorylase.

The phosphate binding site, composed of residues Ser-33, Arg-84, His-86, and Ser-220, is located near a glycine-rich loop (residues 32–37) with the phosphate positioned for nucleophilic attack at atom C(1′) of the nucleoside. The ribose binding site is largely hydrophobic and contains a hydrogen bonding group, Tyr-88, which interacts with the O(3′) position. The residue nearest O(2′) is Met-219 and the residue nearest O(5′) is His-86. One side of the ribose binding site contains several aromatic amino acids including Phe-159, Phe-200, His-86, and Tyr-88. This hydrophobic patch serves to orient the ribose to facilitate nucleophilic attack by phosphate and subsequent inversion at C(1′).

A Swinging Gate Controls Access to the Active Site. The initial electron density for PNP was weak and poorly defined near residues 241–260 (16), indicating high thermal motion for these residues. X-ray analysis of many complexes of PNP with substrates or inhibitors has now confirmed that these residues form a gate that opens during substrate binding to accommodate the substrate or a competitive inhibitor. The maximum movement after substrate or inhibitor binding occurs at His-257, which is displaced outward by several angstroms. The gate is anchored near the central β-sheet at one end and near the C-terminal helix at the other end. The gate movement is complex, apparently involving a helical transformation near residues 257–261. Consequently, initial inhibitor modeling attempts using the native PNP structure were far less successful than subsequent analyses using coordinates for the guanine–PNP complex.

Previously Known PNP Inhibitors. Prior to our studies, several PNP inhibitors had been reported with K_i values of 10^{-6}–10^{-7} including 8-aminoguanine (21), 9-benzyl-8-aminoguanine (22), and 5′-iodo-9-deazainosine (23). Acyclovir diphosphate (24) had a K_i value near 10^{-8} if assayed at 1 mM phosphate rather than the more frequently used value of 50 mM. During our studies, the synthesis of 8-amino-9-(2-thienylmethyl)guanine (K_i, 6.7×10^{-8} M) was reported (25). Complexes of these compounds bound to PNP, which were analyzed by x-ray crystallography, are illustrated in Fig. 4. The most important findings were the following: (*i*) 8-amino substituents enhance binding of guanines by forming hydrogen bonds with Thr-242 and possibly the carbonyl oxygen atom of Ala-116, (*ii*) 9-deaza analogs acquire potency through donation of a hydrogen bond to Asn-243, (*iii*) substitution by hydrophobic groups at the 9-position of a purine enhances binding through interaction with the hydrophobic region in the ribose binding site, (*iv*) acyclovir diphosphate is a multisubstrate inhibitor in which the acyclic spacer between N(9) of the purine and the phosphate is optimal for accommodating the two binding sites, and (*v*) additional binding affinity in acyclovir diphosphate may result from a hydrogen bond between the α-phosphate and Tyr-88 and from the interaction of the ethylene spacer and the hydrophobic region. Based on these results, a number of compounds were proposed that incorporated these and other features predicted to enhance inhibitor binding.

The Hydrophobic Patch in the Ribose Pocket Contributes to Tight Binding Inhibitors. An initial series of compounds synthesized in this program exploited the hydrophobic region in the ribose binding site. A number of 9-substituted 9-deazapurine analogs were prepared with various aromatic, heteroaromatic, and cyclic aliphatic substituents. Crystallographic data showed that generally the planes of the aromatic rings tend to orient in a reproducible conformation. The aromatic groups optimize their interaction with Phe-159 and Phe-200 resulting in the classic herringbone arrangement reported in a variety of aromatic systems (26). In some cases, ring substitution resulted in displacement of the molecular centroid; however, the ring tilt relative to Phe-159 and Phe-200 remained relatively constant. The optimum spacer

FIG. 3. Ball and stick model of key residues in the active site of PNP. Color coding is by atom type with carbon atoms green, oxygen atoms red, and nitrogen atoms blue. Models of guanosine and phosphate that were determined from x-ray crystallographic studies are also shown.

between the purine base and the aromatic substituent appears to be a single methylene group.

Inhibitors with cyclic aliphatic substituents at N(9) were as potent as the aromatic analogs discussed above with the aliphatic substituents occupying the same general volume as the aromatic groups (Table 1). As with the aromatic series, the optimum spacer was one carbon atom. X-ray analysis of the PNP complex of 9-cyclohexyl-9-deazaguanine and the complex of 9-cyclohexylmethyl-9-deazaguanine showed the surprising result that the two cyclohexyl groups occupy approximately the same volume and the 9-deazapurine of the cyclohexyl analog is shifted in order to accommodate the nonoptimal fit to the active site.

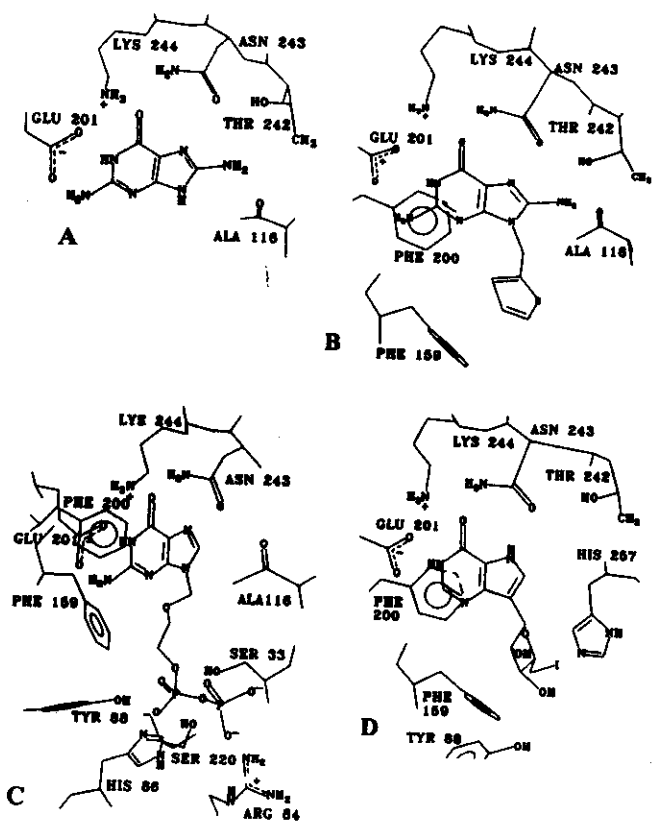

FIG. 4. Line drawings of representative inhibitors in the active site of PNP. The inhibitors are 8-aminoguanine (*A*), 8-amino-9-(2-thienylmethyl)guanine (*B*), acyclovir-diphosphate (*C*), and 5′-iodo-9-deazainosine (*D*). The models were prepared from analysis of difference Fourier maps using 3.2 Å resolution data and calculated phases.

Inhibitor Potency Is Dependent on Phosphate Concentration for a Wide Variety of Compounds. Previously, Tuttle and Krenitsky (24) established that the K_i value for acyclovir diphosphate was larger at 50 mM phosphate (standard assay conditions) than at 1 mM phosphate (cellular conditions) (27). This result can be explained by competition between the distal phosphate group and inorganic phosphate for the phosphate binding site. During our crystallographic analysis of certain PNP–inhibitor complexes, we discovered significant displacements of the inhibitors in the active site that appeared to result from close contacts between the inhibitor and a sulfate ion that occupies the phosphate binding site.

Table 1. Inhibition data for selected PNP inhibitors by increasing IC_{50} value

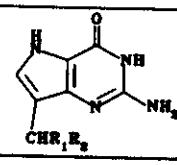

R_1*	R_2	IC_{50}, μM: 50 mM phosphate†	IC_{50}, μM: 1 mM phosphate‡	Ratio§
(*S*)-3-Chlorophenyl	CH_2CO_2H	0.031	0.0059	5.3
3-Chlorophenyl	CH_2CN	1.8	0.010	180
2-Tetrahydrothienyl	H	0.22	0.011	20
3,4-Dichlorophenyl	H	0.25	0.012	21
3-Thienyl	H	0.08	0.020	4.0
3-Trifluoromethylcyclohexyl	H	0.74	0.020	37
Cyclopentyl	H	1.8	0.029	62
Cycloheptyl	H	0.86	0.030	29
Pyridin-3-yl	H	0.20	0.030	7.3
2-(Phosphonoethyl)phenyl¶	H	0.45	0.035	13
Cyclohexyl	H	2.0	0.043	47
2-Furanyl	H	0.31	0.085	3.6
(*R*)-3-Chlorophenyl	CH_2CO_2H	0.90	0.16	5.6
2-Phosphonopropoxyphenyl¶	H	42	1.0	42

*Compounds with R_2 not equal to H are racemic mixtures unless the *R* or *S* isomer is designated.
†Calf spleen PNP assayed in 50 mM phosphate buffer.
‡Calf spleen PNP assayed in 1 mM phosphate buffer.
§IC_{50} at 50 mM phosphate divided by IC_{50} at 1 mM phosphate.
¶Guanine base.

Therefore, we assayed these and other PNP inhibitors at both 1 mM and 50 mM phosphate. These results, summarized in Table 1, show that the IC_{50}(50 mM) is equal to or larger than the IC_{50}(1 mM), in some cases by as much as 100-fold. The ratio and the dimension of the 9-substituent show some correlation. Some compounds, such as 8-aminoguanosine and 8-amino-9-(2-thienylmethyl)guanine, show no difference. In the case of nucleosides, the result may be due to a hydrogen bond between the phosphate and O(3'). Since the concentration of phosphate in intact cells is ≈1 mM, we routinely used this assay condition for all PNP inhibitors.

8-Amino-9-deazaguanine Analogs Are Poor Inhibitors. Both 8-aminoguanine analogs and 9-deazaguanine analogs are good inhibitors of PNP; however, the first 8-amino-9-deazapurine analog prepared was a relatively poor PNP inhibitor. To explain this poor binding, we undertook crystallographic analysis of PNP complexes with four compounds having a 9-thienylmethyl substituent but with the bases being guanine, 8-aminoguanine, 9-deazaguanine, and 8-amino-9-deazaguanine. The results of the x-ray analysis are summarized in Fig. 5. These data showed one binding mode for compounds that accept a hydrogen bond at N(7) and another for compounds that have a hydrogen bond donor at N(7). In both types of binding, a hydrogen bond is formed between N(7) and Asn-243. The 8-aminoguanine analogs make use of the Thr-242 side chain to form an additional hydrogen bond and to improve binding affinity. When N(7) has an attached hydrogen atom, Asn-243 undergoes a shift that is clearly seen in difference Fourier maps and is probably caused by the formation of the highly favorable N(7)-H···O hydrogen bond. A concomitant shift by Thr-242 results in its inability to hydrogen bond to 8-amino substituents. Furthermore, the overall conformational change causes the γ-carbon of Thr-242 to approach the 8-position of the purine, thereby generating a hydrophobic environment for the 8-amino group and causing a decrease in binding affinity. Table 2 lists IC_{50} values for several PNP inhibitors, which exhibit this striking phenomenon.

Branching at the Benzylic Carbon Atom Allows for Optimum Binding of Multisubstrate Inhibitors. To take full advantage of the binding properties of the enzyme active site, it is necessary to design compounds that bind to all three subsites. Acyclovir diphosphate, although not membrane permeable and subject

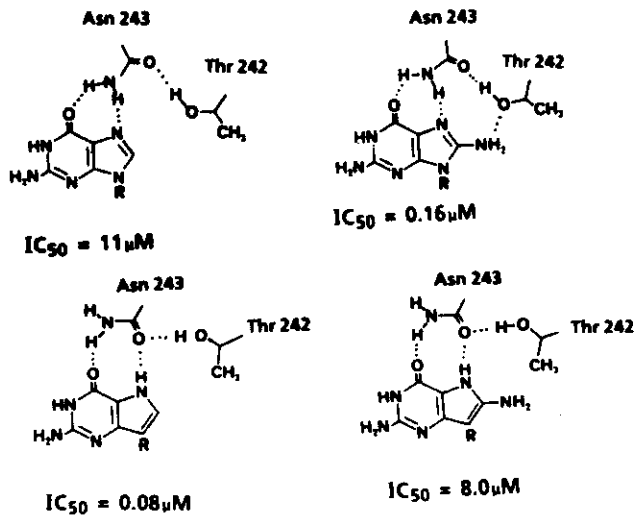

FIG. 5. Comparison of the effects of 8-amino and 9-deaza modifications of purine analogs. The R group is 2-thienylmethyl in the purine example and 3-thienylmethyl in the 9-deazapurine example. Proposed hydrogen bonds, shown as dotted lines, are derived from the analysis of difference Fourier maps. The IC_{50} values are taken from Table 2 at 50 mM phosphate.

Table 2. Effects of 8-amino substitution

9-substituent	IC_{50}, μM			
	G	8-AG	9-DG	8-A-9-DG
2-Thienylmethyl	11*	0.16*	0.14	—
3-Thienylmethyl	—	0.085*	0.08	8.0
Benzyl	—	0.47*	0.23	7.7
Cyclohexylmethyl	—	—	2.2	150
3-Methyl-2-thienyl methyl	48*	4*	—	—
2-Furanylmethyl	18*	0.25*	0.31	—

Calf spleen PNP was assayed in 50 mM phosphate buffer. G, guanine; 8-AG, 8-aminoguanine; 9-DG, 9-deazaguanine; 8-A-9-DG, 8-amino-9-deazaguanine.
*Human erythrocytic PNP assayed in 50 mM phosphate buffer (28).

to extracellular metabolism, is a good example. Our results suggest that an ideal PNP inhibitor in the 9-deazapurine series would contain a bulky hydrophobic group and a substituent with affinity for the phosphate site interlinked by spacers with optimum lengths. Crystallographic and modeling studies suggested a single atom as the optimal spacer between the purine base and hydrophobic group, while modeling studies using coordinates from the native enzyme suggested that a two- to four-atom spacer should link the hydrophobic group to a group having affinity for the phosphate binding site. Such a compound (structure 1) with a four-atom spacer from the ortho position of a benzyl group to a phosphonate group was a surprisingly poor PNP inhibitor.

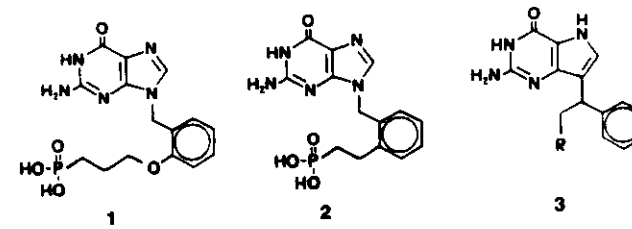

Subsequent crystallographic analysis revealed that the plane of the aromatic ring had rotated ≈90° in order to accommodate the long spacer. More sophisticated modeling studies using coordinates from the guanine–PNP complex and Monte Carlo/energy minimization techniques predicted that a two-carbon spacer would provide a better fit while maintaining the optimum orientation of the aromatic ring. A compound (structure 2) with a two-carbon spacer was a much better inhibitor of PNP; however, it was clear from the x-ray analysis that the aromatic ring was still not able to form an ideal Herringbone packing interaction. Concurrently, compounds (structure 3) were being modeled in which the spacer to the phosphate binding site branched from the benzylic carbon, thus placing no direct restrictions on the tilt of the aromatic ring. Several compounds have now been prepared in this series and confirm the modeling studies based on the x-ray structure. One of the racemic mixtures was separated, individual IC_{50} values were determined, and crystallographic analysis was carried out on the enantiomers. This analysis showed that the *S* isomer is the potent PNP inhibitor. Fig. 6 shows an active site model of the best PNP inhibitor along with the experimental electron density. This series of compounds contains the most potent membrane-permeable inhibitors of PNP yet reported.‖

Summary. Crystallographic and modeling methods have been combined with organic synthesis to produce inhibitors

‖A variety of *in vivo* assays have been performed for the most potent PNP inhibitors. These include evaluation of T-cell cytotoxicity in cell cultures and elevation of inosine levels resulting from PNP inhibition in rats.

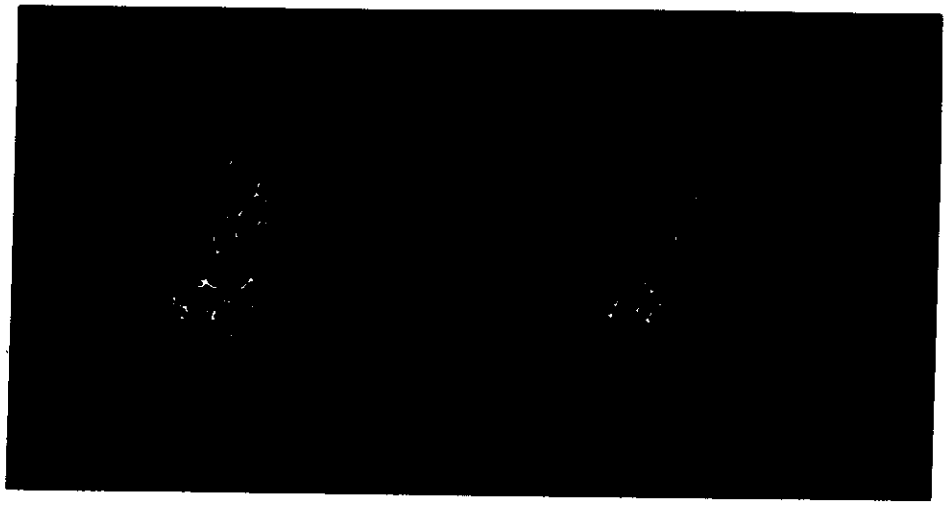

FIG. 6. Binding geometry of the best PNP inhibitor (Table 1, first entry). The difference electron density (complex native) at 3.2 Å resolution is shown for the inhibitor. The key amino acid residues in the active site are shown. The phosphate ion, which would normally be displaced by the inhibitor, is also shown for reference.

of PNP. Kinetic data for selected compounds showed that the inhibitors are competitive with respect to inosine. The approach can best be described as iterative, in which accumulated knowledge is used to produce optimized compounds. Competitive inhibitors benefit from the following features: (*i*) an analog purine base with hydrogen bonds to Glu-201, Thr-242, Asn-243, and/or Lys-244, (*ii*) a bulky hydrophobic group near the ribose binding site, (*iii*) a substituent with affinity for the phosphate binding site, and (*iv*) spacers that link these groups together without perturbing the binding geometry of the individual groups. These features are exemplified in compounds such as (*S*)-9-[1-(3-chlorophenyl)-2-carboxyethyl]-9-deazaguanine (Table 1, first entry), which exhibits an IC_{50} value of 5.9 nM.

We found that computer modeling required significant tuning in order to provide useful results. Crystallographic results were useful in testing and modifying modeling parameters. The most useful modeling results were achieved after incorporation of the conformational searching techniques described above and when the coordinates for the PNP–guanine complex model were used.

Crystallographic analysis was based primarily on the results of difference Fourier maps in which the quantitative relationships between residues in the active site and the inhibitor could be characterized. During these studies, ≈35 PNP–inhibitor complexes were evaluated by x-ray crystallographic techniques. It is noteworthy that the resolution of the PNP model extends to only 2.8 Å and that all of the difference Fourier maps were calculated at 3.2 Å resolution, much lower than often considered essential for drug design. Crystallographic analysis was facilitated by the large solvent content that allowed for free diffusion of inhibitors into enzymatically active crystals (28). During the 2.5 years of this project, ≈60 active compounds were synthesized. The large number of active compounds designed and the enhancement in inhibitor potency of nearly 2 orders of magnitude stand as proof that crystallographic and computer-assisted modeling methods are now capable of playing a critical role in the rapid discovery of therapeutic agents.

We thank Dr. S. Narayana, Dr. W. Cook, Dr. M. Carson, and Mrs. C. Woodruff of the University of Alabama at Birmingham; Drs. S. Niwas, R. Elliot, J. Rose, S. Ananthan, L. Bennett, and P. Allen of the Southern Research Institute; Drs. M. Allen, F. Clarke, and J. Stanton of CIBA-Geigy; Drs. J. Stoeckler and R. Parks, Jr., of Brown University; Drs. J. Tuttle and T. Krenitsky of Burroughs Wellcome. This research was supported by grants from the American Cancer Society (CH-213), the Leukemia Society of America, the National Institutes of Health (GM-38823), and the National Aeronautics and Space Administration (NAGW-813 and NAS8-36611).

1. Erickson, J., Neidhart, D. J., VanDrie, J., Kempf, D. J., Wang, X. C., Norbeck, D. W., Plattner, J. J., Rittenhouse, J. W., Turon, M., Wideburg, N., Kohlbrenner, W. E., Simmer, R., Helfrich, R., Paul, D. A. & Knigge, M. (1990) *Science* **249**, 527–533.
2. McCammon, J. A. & Harvey, S. C. (1987) *Dynamics of Proteins and Nucleic Acids* (Cambridge Univ., New York).
3. Van Gunsteren, W. F. & Weiner, P. K., eds. (1989) *Computer Simulation of Biomolecular Systems: Theoretical and Experimental Applications* (Escom Science, Leiden, The Netherlands).
4. Stoeckler, J. D. (1984) in *Developments in Cancer Chemotherapy*, ed. Glazer, R. E. (CRC, Boca Raton, FL), pp. 35–60.
5. Friedkin, M. & Kalckar, H. (1961) in *The Enzymes*, eds. Boyer, P. D., Lardy, H. & Myrback, K. (Academic, New York), 2nd Ed., Vol. 5, pp. 237–255.
6. Parks, R. E., Jr., & Agarwal, R. P. (1972) in *The Enzymes*, ed. Boyer, P. D. (Academic, New York), 3rd Ed., Vol. 7, pp. 483–514.
7. Agarwal, K. C., Agarwal, R. P., Stoeckler, J. D. & Parks, R. E., Jr. (1975) *Biochemistry* **14**, 79–84.
8. Bzowska, A., Kulikowska, E. & Shugar, D. (1990) *Z. Naturforsch. C: Biosci.* **45**, 59–70.
9. Stoeckler, J. D., Agarwal, R. P., Agarwal, K. C., Schmid, K. & Parks, R. E., Jr. (1978) *Biochemistry* **17**, 278–283.
10. Williams, S. R., Goddard, J. M. & Martin, D. W., Jr. (1984) *Nucleic Acids Res.* **12**, 5779–5787.
11. LePage, G. A., Junga, I. G. & Bowman, B. (1964) *Cancer Res.* **24**, 835–840.
12. Erion, M. D. (1990) *Eur. Patent Appl.* 374,096.
13. Giblett, E. R., Ammann, A. J., Wara, D. W., Sandman, R. & Diamond, L. K. (1975) *Lancet* **i**, 1010–1013.
14. Sircar, J. C. & Gilbertsen, R. B. (1988) *Drugs of the Future* **13**, 653–668.
15. Stoeckler, J. D., Ealick, S. E., Bugg, C. E. & Parks, R. E., Jr. (1986) *Fed. Proc. Fed. Am. Soc. Exp. Biol.* **45**, 2773–2778.
16. Ealick, S. E., Rule, S. A., Carter, D. C., Greenhough, T. J., Babu, Y. S., Cook, W. J., Habash, J., Helliwell, J. R., Stoeckler, J. D., Parks, R. E., Jr., Chen, S.-F. & Bugg, C. E. (1990) *J. Biol. Chem.* **265**, 1812–1820.
17. Mohamadi, F., Richards, N. G. J., Guida, W. C., Liskamp, R., Lipton, M., Caufield, C., Change, G., Hendrickson, T. & Still, W. C. (1990) *J. Comput. Chem.* **11**, 440–467.
18. Weiner, S. J., Kollman, P. A., Case, D. A., Singh, U. C., Ghio, C., Alagona, S., Profeta, S. & Weiner, P. (1984) *J. Am. Chem. Soc.* **106**, 765–784.
19. Weiner, S. J., Kollman, P. A., Nguyen, T. D. & Case, D. A. (1986) *J. Comput. Chem.* **7**, 230–252.
20. Chang, G., Guida, W. C. & Still, W. C. (1989) *J. Am. Chem. Soc.* **111**, 4379–4386.
21. Stoeckler, J. D., Cambor, C., Kuhns, V., Chu, S.-H. & Parks, R. E., Jr. (1982) *Biochem. Pharmacol.* **31**, 163–171.
22. Shewach, D. S., Chern, J.-W., Pillote, K. E., Townsend, L. B. & Daddona, P. E. (1986) *Cancer Res.* **46**, 519–523.
23. Stoeckler, J. D., Ryden, J. B., Parks, R. E., Jr., Chu, M.-Y., Lim, M.-I., Ren, W.-Y. & Klein, R. S. (1986) *Cancer Res.* **46**, 1774–1778.
24. Tuttle, J. V. & Krenitsky, T. A. (1984) *J. Biol. Chem.* **259**, 4065–4069.
25. Gilbertsen, R. B., Scott, M. E., Dong, M. K., Kossarek, L. M., Bennett, M. K., Schrier, D. J. & Sircar, J. C. (1987) *Agents Actions* **21**, 272–274.
26. Burley, S. K. & Petsko, G. A. (1985) *Science* **229**, 23–28.
27. Castleman, B. & McNeely, B. U., eds. (1974) *N. Engl. J. Med.* **290**, 39–49. 653.
28. Ealick, S. E., Babu, Y. S., Narayana, S. V. L., Cook, W. J. & Bugg, C. E. (1990) in *Advances in Chemotherapy of AIDS*, eds. Diasio, R. B. & Sommadossi, J.-P. (Pergamon, New York), pp. 97–108.
29. Appelt, K., Bacquet, R. J., Bartlett, C. A., Booth, C. L. J., Freer, S. T. *et al.* (1991) *J. Med. Chem.* **34**, 1925–1934.